Hydrogen-poor core-collapse supernovae

Elena Pian and Paolo A. Mazzali

Abstract Hydrogen-poor core-collapse supernovae signal the explosive death of stars more massive than the progenitors of hydrogen-rich core-collapse supernovae, i.e. approximately in the range 15–50 $M_{\odot}$ in main sequence. Since hydrogen-poor core-collapse supernovae include those that accompany gamma-ray bursts, which were all rigorously identified with type Ic supernovae, their explosion energies cover almost two decades. The light curves and spectra are consequently very heterogeneous and often bear the signature of an asymmetric, i.e. aspherical, explosion. Asphericity is best traced by early-time (within days of the explosion) optical spectropolarimetry and by late epoch (more than $\sim$100 days after explosion) low-resolution spectroscopy. While the relationship between hydrogen-poor core-collapse supernovae to hydrogen-poor super-luminous supernovae is not understood, a known case of association between an ultra-long gamma-ray burst and a very luminous hydrogen-poor supernova may help unraveling the connection. This is tantalizingly pointing to a magnetar powering source for both phenomena, although this scenario is still highly speculative. Host galaxies of hydrogen-poor supernovae are always star forming; in those of completely stripped supernovae and gamma-ray burst supernovae, the spatial distribution of the explosions follows the blue/ultraviolet light, with a correlation that is more than linear.

Elena Pian
INAF-IASF, Via P. Gobetti 101, I-40129 Bologna, Italy, and Scuola Normale Superiore, Piazza dei Cavalieri 7, I-56126, Pisa, Italy, e-mail: elena.pian@sns.it

Paolo A. Mazzali
Astrophysics Research Institute, Liverpool John Moores University, IC2, Liverpool Science Park, 146 Brownlow Hill, Liverpool L3 5RF, UK, e-mail: P.Mazzali@ljmu.ac.uk

1 Introduction

Most of the supernova (SN) light is emitted in optical, and is due to radioactive decay of ^{56}Ni, with a possible contribution from a different component, an active inner rotating and/or accreting compact star, often referred to in the literature as an "engine". Unlike thermonuclear SNe (with only one member of this class possibly detected in X-rays, Immler et al. 2006), core-collapse SNe are sometimes detected at radio and X-ray wavelengths. In hydrogen-poor SNe, the radio and X-ray emission observed days or months after explosion is often due to synchrotron and inverse Compton process, respectively (Chevalier & Fransson 2006).

Owing to its overwhelming importance, we will mainly concentrate here on the optical (including near-infrared and near-ultraviolet) display of hydrogen-poor SNe – light curves (Section 3) and spectra (Section 4) – that accounts for more than 90% of the observed bolometric luminosity in core-collapse SNe. Section 5 presents a recently detected example of an ultra-long GRB associated with a peculiar hydrogen-poor SN, which constitutes the first discovered case of a possibly rare sub-group of objects, still almost completely unexplored. In Section 6 the close environments and host galaxies of hydrogen-poor SNe are reviewed. Section 7 will draw a summary and outlook on future research in this field. The present chapter does not cover hydrogen-poor super-luminous SNe.

2 Stripped-envelope core-collapse supernovae

Core-collapse SNe that have little or no hydrogen and helium in their envelopes (i.e. types Ib, Ic, and IIb), called hydrogen-poor or stripped-envelope SNe, are probably associated with more massive stars than the progenitors of type II SNe, i.e. Wolf-Rayet stars of various composition (Crowther 2007). They have to be sufficiently massive to shed most of their hydrogen and part of their helium envelopes. Possible observational evidences of Wolf-Rayet progenitors of stripped-envelope SNe come from pre-explosion images of a very few progenitor star candidates, as opposed to many type II SNe with direct progenitor identification (Smartt 2009). Early spectroscopy may also reveal the properties of the exploding star, as in the case of type IIb SN 2013cu, where the characteristic emission lines of a Wolf-Rayet stellar wind interacting with the SN radiation field were detected (Gal-Yam et al. 2014).

The stripping of hydrogen and helium envelopes in massive stars is due both to winds (Owocki et al. 2009) and, most frequently, to binarity (Smith 2014). Remarkably, the number of Ib SNe (i.e. hydrogen-poor but helium-rich) is relatively scarce with respect to Ic (stripped of both hydrogen and helium) and IIb (which keep some traces of hydrogen), as if helium-stripping only came in two extreme modes, either negligible or complete (Benetti et al. 2011; Hachinger et al. 2012). Chevalier & Soderberg (2010) propose a further subdivision of IIb SNe in extended-envelope and compact-envelope events based on a mass of hydrogen larger or smaller than

$\sim$0.1 $M_\odot$, respectively. A particular subgroup of Ic SNe is represented by those connected with gamma-ray bursts (GRBs). These are the subject of sub-section 2.1.

2.1 Gamma-ray burst supernovae

GRBs are extragalactic transient sources occurring at a rate of about 1 per day, as observed by gamma-ray missions in the last twenty years (CGRO/Batse, BeppoSAX/GRBM, Swift/BAT, Fermi/GBM). They outshine the soft-gamma-ray sky at their peak emission, have bright multi-wavelength afterglows, faint, star-forming host galaxies and most likely owe their phenomenology to highly collimated ultra-relativistic outflows (MacFadyen & Woosley 1999; Mészáros 2002). The majority of observed GRBs have durations longer than $\sim$2 s (Kouveliotou et al. 1993) and are thus defined as long GRBs, as opposed to short or sub-second GRBs. The long GRB class includes X-ray flashes, characterized by softer spectra than those of GRBs: typically, the integrated spectrum of a "classical" GRB peaks around 100-1000 keV, while the spectra of X-ray flashes peak at 5-10 keV (Sakamoto et al. 2008).

Virtually all long GRBs and X-ray flashes are accompanied by type Ic SNe with broad absorption lines. The prototype and best studied is the closest one, SN 1998bw (35 Mpc) associated with GRB980425 (Galama et al. 1998; Kulkarni et al. 1998; Pian et al. 2000). At redshift $z < 0.2$, the signal-to-noise ratio of the optical spectroscopy of GRB SNe is sufficiently high that individual absorption features can be identified and unambiguous typing is possible. This is the case for another five GRB SNe: SN 2003dh, SN 2003lw, SN 2006aj, SN 2010bh, SN 2013dx (Woosley & Bloom 2006; D'Elia et al. 2015, and references therein).

At higher redshifts, the contamination of the host galaxy and of afterglow light in the optical makes the identification of absorption lines impossible, and the evidence for the presence of a SN is based only on a general resemblance of the spectral shape of the GRB optical counterpart with that of known GRB SNe and on the rebrightening of the optical light curve at a time interval from GRB explosion compatible with SN maximum light (e.g., Melandri et al. 2014). Their association with type Ic SNe implies that long GRB progenitors must be bare, highly stripped cores of massive stars (although not the most massive ones). In a single star this stage may be reached if mass is shed through a wind, which however also removes angular momentum, inhibiting the conditions for jet formation. A binary companion may instead enable mass transfer more efficiently, with no loss of angular momentum (Izzard et al. 2004). Progenitor main sequence masses of hydrogen-poor core-collapse SNe estimated from modelling of light curves and spectra (see Section 4.1) range between 15 and 50 $M_\odot$ (Mazzali et al. 2013). Evolutionary models of single stars predict a lower limit on the Ib/c SNe progenitor masses of 20-25 $M_\odot$ (Heger et al. 2003), where the small discrepancy with respect to radiative transfer modelling results can be attributed to stellar binarity.

Two competing models for the formation of long GRBs are currently under consideration, both of which rely on the formation of a relativistic jet after the collapse

of a massive stellar core. The collapsar scenario (MacFadyen & Woosley 1999) envisages accretion of stellar material with a very high rate ($\sim$0.1 $M_\odot$ s^{-1}) on a black hole formed promptly after a rapid proto-neutron star phase. An alternative model involves the formation of a rapidly spinning (with millisecond period), highly magnetized neutron star (magnetar) that drives and powers a mildly relativistic outflow. This produces a bipolar jet that is magnetically accelerated and collimated and breaks out of the stellar surface with ultra-relativistic speed (Duncan & Thompson 1992; Metzger et al. 2015). This rotation-powered proto-magnetar scenario provides a rotational energy of $\sim 10^{52}$ erg and magnetic-dipole luminosity of $\sim 10^{51}$ erg s^{-1}, suitable to account for the typical observed kinetic energies of GRB SNe and apparent (i.e. isotropic-equivalent) energies and peak luminosities of GRBs (Usov 1992; Woosley & Bloom 2006; Kasen & Bildsten 2010). A magnetar was proposed to explain the second of two light maxima observed in the type Ib SN 2005bf (Maeda et al. 2007), although other interpretations are viable (Folatelli et al. 2006).

3 Light curves

Large compilations of optical and ultraviolet light curves of stripped-envelope SNe were reported by Li et al. (2011), Pritchard et al. (2014), and Prentice et al. (2016), among others. Their shape is generally similar to that of type Ia SNe, but the luminosities are lower and cover a much wider interval, about 3 magnitudes (Figure 1). The colors span a similarly wide range (Prentice et al. 2016). Unlike type Ia SNe, type I core-collapse SNe do not exhibit any strong correlation between the peak luminosity and the width of the light curve, although the most luminous of them tend also to have a broader peak as a consequence of their larger mass, larger opacities, and diffusion times. A rapid rise often signals significant asymmetry in the explosion, which is better explored and confirmed from the analysis of the nebular phase spectra (see Section 4.2). Using well sampled SN light curves (particularly with good data coverage around light curve maximum) one can estimate the amount of synthesized ^{56}Ni with the aid of radiative transport models (see e.g. Hoeflich et al. 1993; Cappellaro et al. 1997; Kasen & Plewa 2007). For "normal" Ib/c SNe (i.e. not accompanied by a high energy transient) and X-ray flashes SNe this is usually of the order of 0.1-0.2 $M_\odot$. SNe associated with "regular" GRBs synthesize typically more ^{56}Ni (SN 1998bw has an estimated ^{56}Ni mass of 0.35 $M_\odot$, Mazzali et al. 2006).

When core-collapse SNe are discovered within days of the explosion, it is occasionally possible to detect an initial optical/ultraviolet flare of thermal nature – or the decaying phase thereof – due to shock break-out. In stripped-envelope core-collapse SNe shock break-out emission is more rapid than in type II SNe, because of the absence of a massive hydrogen reprocessing envelope, and more difficult to observe. In the two nearby SNe 2006aj and 2010bh associated with X-ray flashes the shock break-out component may have been seen also in X-rays (Campana et al. 2006; Starling et al. 2011), although the interpretation of this emission is controversial, alternatives pointing to non-thermal emission (Ghisellini et al. 2007; Waxman

et al. 2007). A similar controversy affects the early ultraviolet/X-ray emission accompanying the type Ib SN 2008D, that was serendipitously detected by *Swift* while observing the field of the nearby galaxy NGC2770 (Soderberg et al. 2008; Mazzali et al. 2008).

4 Spectra

Wide field and high cadence optical surveys and rolling searches are currently detecting a large number of SNe soon (a few days or even hours) after explosion. Early spectroscopy, made possible by flexible small optical and near-infrared telescopes on the ground and in the ultraviolet by the UVOT instrument onboard *Swift*, and early radio and X-ray follow-up are thus mapping the initial expansion of the ejecta and providing unprecedented information on the close circumstellar medium and details on the progenitor. Larger aperture (8-10m) telescopes are then used to follow the later SN stages and the transition of the ejecta from photospheric to nebular phase, characterized by extremely low flux levels. The properties of core-collapse stripped-envelope SNe were reviewed by Filippenko (1997), Matheson et al. (2001), and Modjaz et al. (2014), based on vast collections of time-resolved spectra of increasing numbers of sources. A comprehensive and interactive database of SN spectra, including hydrogen-poor SNe, is maintained at the Weizmann Institute of Science (WISeREP, Yaron & Gal-Yam 2012, http://wiserep.weizmann.ac.il).

In the first months after explosion, SN spectra are dominated by absorption lines due to atomic species in the outer ejecta. The ejecta become increasingly transparent with time and their inner regions, closer to the explosion site, are progressively exposed. In stripped-envelope core-collapse SNe, starting $\sim$100 days after explosion, the conditions of increasing transparency in the ejecta allow the formation of emission lines, mostly forbidden, which bear the signature of the explosion geometry and trace its degree of anisotropy. In sub-sections 4.1 and 4.2 the main results of stripped-envelope SN spectroscopy in photospheric and nebular phase are reported, respectively.

4.1 Photospheric phase

In the early phases after gravitational collapse and explosion, SN ejecta are optically thick, and the continuum spectrum from the near-infrared to near-ultraviolet can be approximated by a black body, barring superposed emission due to interaction of the SN shock with the circumstellar medium. The temperature decreases with time (with ejecta expansion and shock cooling) and absorption lines form above the photosphere, signalling the presence of lowly ionized atomic species whose abundances point to the composition of the star at pre-SN stage. The spectrum is suppressed by line blanketing, the severity of which is related to the amount of iron-group ele-

ments, and to the level of line-broadening caused by the ejecta velocity. Figure 2 (left panel) shows individual examples of the four main types of hydrogen-poor core-collapse SNe, although we note that an event within the hydrogen-poor group may morph in time from one type to the other. Near-ultraviolet spectroscopy of hydrogen-poor SNe is made difficult by the intrinsically low flux levels and the suppression caused by line-blending in this spectral range. Only the brightest events have ultraviolet spectra observed by *IUE*, *HST*, or *Swift*/UVOT (Jeffery et al. 1994; Bufano et al. 2009; Ben-Ami et al. 2015). The near-infrared spectral region may be critical to determine the amount of helium present in the ejecta, because the He absorption I line at 2.058 μm is typically uncontaminated by other lines (e.g., Taubenberger et al. 2006).

Ejecta expansion velocities can be measured from the spectra or derived through the application of models to the observed spectra (see below). Speeds obtained with the latter method are more reliable because they are not affected by possible line blending. For this reason, when measuring velocities directly from the spectra, it is necessary to use lines that are relatively isolated and free from contamination by other lines. The Doppler-shifted wavelength of the minimum of a given (observed or modeled) absorption line profile gives the photospheric speed; the higher the speed, the more broadened are the lines, because of the larger distribution of velocities (left panel of Figure 2). Typical velocities for stripped-envelope core-collapse SNe around maximum luminosity range between a few thousands of km s^{-1}, as in SN 1994I, to very broad lines ($\sim$60000 km s^{-1}, as in SN 2002ap), and decrease with time (right panel of Figure 2).

The physical parameters of SNe (radioactive ^{56}Ni mass, kinetic energy, ejecta mass, composition, progenitor and remnant mass) can be estimated via models based on radiative transport and Monte Carlo methods to approximate the photon diffusion in the SN ejecta (Nakamura et al. 2001; Mazzali et al. 2006). From the SN spectra, chemical abundances, ejecta mass and kinetic energy are determined; coupling this information with the bolometric light curve, a synthetic light curve is computed that provides an estimate of the synthesized ^{56}Ni mass (see also Arnett 1982). From the ejecta and ^{56}Ni masses, the mass of the collapsing core can be estimated and the evolution can be traced back to the main sequence by using the stellar evolution models (e.g. Nomoto & Hashimoto 1988).

In GRB SNe (see Section 2.1), it is customary to observe velocities above 30000 km s^{-1} during the first 10 days after explosion (Galama et al. 1998; Nakamura et al. 2001; Mazzali et al. 2006; D'Elia et al. 2015). Combined with the high ejecta masses, these velocities imply kinetic energies of more than 10^{52} erg, well in excess of the typical value of 10^{51} erg that represents the characteristic total kinetic energy of a SN (of any type). The kinetic energies of broad-lined SNe not accompanied by GRBs are never as high as those of GRB SNe (Mazzali et al. 2013), suggesting that a very high initial kinetic energy is a fundamental requirement for the formation of a high-energy transient simultaneous with a core-collapse SN.

Finally, for bright sources, imaging polarimetry and spectro-polarimetry can effectively help investigate the SN expansion geometry and the element distribution, respectively (Kawabata et al. 2003; Gorosabel et al. 2006; Tanaka et al. 2009).

4.2 Nebular phase

During this phase, the continuum emission (once the background galaxy emission is subtracted) vanishes and the spectrum is dominated by forbidden emission lines due to oxygen, carbon, iron, magnesium and Balmer lines in IIb SNe. The left panel of Figure 3 shows a comparison of nebular spectra of different types of SNe. Nebular spectroscopy at low spectral resolution ($\lambda/\Delta\lambda \simeq 600$) is an ideal tool to determine the physical quantities of SNe independently from the photospheric observables, map the chemical abundances of the progenitor, determine the nature of the exploding star, and to study the SN asymmetries, that can be related either to intrinsic asphericities of the explosion (Mazzali et al. 2005) or to dust or rings in the ejecta (Milisavljevic et al. 2012).

Observations of emission lines of iron (which results from the decay of ^{56}Ni) in several bright broad-lined Ic SNe and of the GRB SNe 1998bw and 2006aj (the only two GRB SNe for which spectroscopy in fully nebular phase was possible, thanks to their closeness) have constrained the total synthesized ^{56}Ni mass to values consistent with those obtained from early epoch model analysis (Mazzali et al. 2001,2007), excluding the role of a magnetar as a power source of the light curve (although it could power the explosion itself).

While optical spectro-polarimetry is ideal to study SN asymmetries, the required signal-to-noise ratio and the various systematics limit this technique to very bright and nearby sources. At lower flux levels, nebular spectroscopy is better suited for the search of asphericities in the velocity fields. In the case of the nearest GRB SN, 1998bw, spectra in the nebular phase showed broad [FeII] features coexisting with a narrow [O I] 6300,6363 Å line. This can only be understood if iron moves in the direction of the observer, while oxygen (which is produced during the evolution of the star before explosion and should be located further out in the star) moves more tangentially (Mazzali et al. 2005). This situation can be realised if the SN kinetic energy is injected preferentially along a specific direction, which coincides with the orientation of the GRB. Maeda et al. (2002) showed, using 2D models, that for SN 1998bw we must have observed this aspherical explosion within $\sim 10-15$ degrees of the axis of highest energy injection, which can be identified with the direction of the GRB jet. Neither X-ray flash SNe nor broad-lined Ic SNe not accompanied by GRBs have shown this peculiar emission-line behaviour so far (Mazzali et al. 2007; Maeda et al. 2008), suggesting that they are less aspherical than GRB SNe.

Given this indirect evidence, and since GRBs are rather narrowly collimated events, we should expect a relatively large number of off-axis GRB SNe to be observed. However, this predicted population has not been uncovered yet. The search for off-axis events relies either on nebular spectroscopy or on radio observations. An off-axis GRB SN should show an [O I] line with strong and widely separated double peaks, reflecting the large overall expansion velocities of the ejecta. Radio emission is supposed to be caused by the slowing down of the GRB jet as it interacts with circumstellar material, and since it is isotropic radio observations should pick

up off-axis jets. Radio emission was detected for the nearest GRB SN, SN 1998bw (Kulkarni et al. 1998).

Additionally, it is not clear whether the development of double-peaked [O I] profiles and of radio emission is necessarily simultaneous. SN 2003jd is the only SN Ic which was claimed to be an off-axis GRB SN based on the profile of the [O I] line, where the two components had a velocity separation of ~ 7000 kms (Figure 3, right panel). Note that none of the many other cases of double-peaked [O I] profiles presented in the literature (e.g., Maeda et al. 2008; Maurer et al. 2010) show a wide peak separation, suggesting that no other off-axis GRB SN candidate has been identified. However, no radio emission was found for SN 2003jd (Soderberg et al. 2006) suggesting that if a jet was present it may have been weak (although the observations were not performed late enough to follow the thermalization process of the jet fully). On the other hand, SN 2009bb was claimed to be an off-axis GRB SN based on a radio detection, but nebular spectra did not reveal any signature of asphericity (Pignata et al. 2011): the radio emission may just have been caused by the deceleration of fast but spherical ejecta in the circumstellar medium, but again no GRB may have been present. An off-axis GRB SN should show both of these features. However, most GRB SNe are too far for both of these techniques to be applicable, suggesting that perhaps the lack of candidate detection is just the result of the small volume that can be explored.

5 A link between GRB-supernovae and super-luminous supernovae

The *Swift* satellite has detected an observationally rare class of GRBs, whose duration of about 10000 seconds exceeds significantly the average duration of long GRBs (Boër et al. 2015). The afterglow of one of these "ultra-long" GRBs, GRB111209A, was thoroughly studied at X-ray and optical wavelengths, and the regular and intensive optical/near-infrared monitoring with the GROND instrument on the ESO 2.2m telescope revealed the presence of a SN, SN 2011kl (Greiner et al. 2015). SN 2011kl does not resemble any of the GRB SNe previously detected, being more luminous (about a factor of 3 more luminous than SN1998bw at light curve maximum) and very poor in metals. Its luminosity places it at halfway between "classical" GRB SNe and the so called super-luminous SNe (see Figure 4), a class of SNe recently discovered, very massive and luminous, a fraction of which may be related to pair instability in the stellar nucleus (Gal-Yam 2012). In fact, the spectrum of SN 2011kl is similar to those of super-luminous SNe.

While the light curve can be fitted equally well assuming a magnetar or radioactive ^{56}Ni as a powering source, with the former only marginally favored (Fig. 4), it is the striking similarity of the spectrum of SN2011kl to those of super-luminous SNe, rather than type Ic SNe, that suggests a magnetar interpretation, already proposed for super-luminous SNe (Woosley 2010). The fact that SN 2011kl is more luminous than the other GRB SNe and thus more similar to super-luminous SNe also points to

this scenario. Since the accretion rates implied in a collapsar scenario are incompatible with the GRB duration (the progenitor core mass would exceed many hundreds of solar masses), the magnetar alternative seems viable and even more cogent than it is for the SNe accompanying "regular" long GRB.

6 Host galaxies of stripped-envelope core-collapse supernovae

All core-collapse SNe are found in late-type galaxies or star-forming regions of elliptical galaxies, regardless of whether they are hydrogen-rich or hydrogen-poor (Leaman et al. 2011). While type Ib and Ic SNe tend to favour bright galaxies as hosts, type IIb and broad-lined Ic SNe are predominantly found in dwarf galaxies ($M_r \geq -18$, Arcavi 2012). This is interpreted to be consistent with the fact that the degree of envelope stripping (Ib/c vs IIb) correlates with metallicity, but also calls for the action of an extra mechanism that allows some stars to undergo extensive stripping and explode as broad-lined SNe Ic, occasionally accompanied by long-duration GRBs (Section 2.1).

Kelly et al. (2008) found that once the contribution from the bright bulge is subtracted from their host galaxy images, the distribution of Ic SNe (normal and broad-lined) with respect to the light of their hosts is different from that of type II and Ib, i.e. Ic SNe are more concentrated on the brightest regions of their hosts (Figure 5). This more-than-linear correlation of point-like source distribution and host galaxy rest-frame ultraviolet light is typical also in long GRBs, as determined previously by Fruchter et al. (2006), who first noted also a morphological difference between the hosts of long GRBs and those of core-collapse SNe as a whole population within the same volume ($z < 1.2$). The ensuing implication that more stripped SNe arise from more massive progenitor stars than hydrogen-rich SNe is supported by the fact that type Ib/c SNe are found to occur nearer to bright HII regions than type II SNe, as traced by Hα emission (Anderson et al. 2012).

Progenitor differences in various sub-types of core-collapse SNe point to the possible role of metallicity in determining the evolution of massive stars. This has been studied both on a local scale, with spectroscopy acquired at the explosion site, and on a global scale, via the exploration of integrated properties of the host galaxies. Modjaz et al. (2011) examined the local chemical abundances at the locations of 35 SNe and found that Ib SNe have lower metallicities than Ic SNe, with broad-lined Ic SNe having intermediate metallicities between the two groups.

Kelly & Kirshner (2012) examined SDSS images and spectra of the host galaxies of 519 nearby SNe, finding that broad-lined Ic SNe hosts show lower average oxygen abundances than those of normal Ic SNe. Type IIb SNe host spectra are also more metal-poor than those of SNe Ib. The comparison of the host galaxies of 245 core-collapse SNe at $z < 0.2$, including 17 broad-lined Ic SNe discovered by galaxy-untargeted searches, and 15 optically luminous and dust-obscured $z < 1.2$ long GRBs shows that, in comparison with SDSS galaxies having similar stellar masses, the hosts of the broad-lined Ic SNe and of the GRBs have high surface

densities of stellar mass and star formation rate. Core-collapse SNe having typical ejecta velocities, in contrast, show no preference for such galaxies. It appears that this difference cannot be attributed to a preference for low metal abundances, but must reflect the influence of a separate environmental factor (Kelly et al. 2014). Moreover, the hosts of broad-lined Ic SNe, unlike those of normal Ib/c and II SNe, exhibit high gas velocity dispersions for their stellar masses. This may suggest efficient formation of massive binary progenitor systems in densely star-forming regions.

7 Conclusions

The wide spread of maximum luminosities and variety of light curve shapes and of spectra of hydrogen-poor SNe testifies to their broad range of properties, ultimately related to the diversity of progenitor masses, rotation rates and multiplicity. There is no doubt that the association of the most heavily stripped variety of these SNe, type Ic, with GRBs has boosted the interest and the exploration of these objects, that were very poorly known before the late nineties. The kinetic energies of stripped-envelope SNe may be exceptionally high (more than 10^{52} erg), and they exceed by at least an order of magnitude the collimation-corrected energies of long GRBs (i.e. the observed gamma-ray energy output corrected for the jet aperture), so that in a GRB-SN event, the energetics of the SN dominates the total energy budget. SN asymmetries, whose evidence was found in polarized photospheric spectra and in late epoch emission line spectral profiles, are predicted by explosion models and are presumably conducive to the formation of anisotropic jetted structures whereby relativistic outflows can develop. Indeed, the bare stellar cores that characterize type Ic SNe appear more favourable to the outbreak and unhindered propagation of a GRB ultra-relativistic jet (Lorentz factor $\Gamma \sim 100$) than the massive envelopes of Type II SNe, that would quench the jet rapidly. However, the mechanism that is responsible for jet production, collapsar or magnetar, is not clear and it is here that our knowledge must still make progress.

Super-luminous SNe and their association with ultra-long GRBs compound the issue, but they may also be the key to the final interpretation paradigm. From the observational point of view, hydrogen-poor SN research has acquired large impetus from the many surveys and rolling searches that have made their discovery more efficient and, thanks to regular scans and intensive cadences, have allowed SNe to be detected at increasingly early phases. This is critical for accurate sampling of the early shock break-out component and to constrain the possible time interval between the SN explosion and GRB event. Optical surveys like the intermediate PTF, Pan-STARRS, La Silla Quest, DES, PESSTO, to name only a few, and, in the near future, the Zwicky Transient Facility and LSST will advance SN science and disclose crucial information on the explosions and on their close environments.

8 Cross-References

1. Observational Classification of Supernovae.
2. H-rich core collapse supernovae.
3. Superluminous supernovae

References

1. Anderson, J. P., Habergham, S. M., James, P. A., & Hamuy, M. 2012, MNRAS, 424, 1372
2. Arcavi, I. 2012, Death of Massive Stars: Supernovae and Gamma-Ray Bursts, IAUS 279, 34, Eds. P. Roming, N. Kawai, E. Pian
3. Arnett, W. D. 1982, ApJ, 253, 785
4. Ben-Ami, S., Hachinger, S., Gal-Yam, A., Mazzali, P. A., Filippenko, A. V., Horesh, A., et al. 2015, ApJ, 803, 40
5. Benetti, S., Turatto, M., Valenti, S., Pastorello, A., Cappellaro, E., Botticella, M. T., et al. 2011, MNRAS, 411, 2726
6. Boër, M., Gendre, B., & Stratta, G. 2015, ApJ, 800, 16
7. Bufano, F., Immler, S., Turatto, M., Landsman, W., Brown, P., Benetti, S., et al. 2009, ApJ, 700, 1456
8. Campana, S., Mangano, V., Blustin, A. J., Brown, P., Burrows, D. N., Chincarini, G., et al. 2006, Nature, 442, 1008
9. Cappellaro, E., Mazzali, P. A., Benetti, S., Danziger, I. J., Turatto, M., della Valle, M., & Patat, F. 1997, A&A, 328, 203
10. Chevalier, R. A., & Fransson, C. 2006, ApJ, 651, 381
11. Chevalier, R. A., & Soderberg, A. M. 2010, ApJ, 711, L40
12. Crowther, P. A. 2007, ARA&A, 45, 177
13. D'Elia, V., Pian, E., Melandri, A., D'Avanzo, P., Della Valle, M., Mazzali, P. A., et al. 2015, A&A, 577, A116
14. Duncan, R. C., & Thompson, C. 1992, ApJ, 392, L9
15. Filippenko, A. V. 1997, ARA&A, 35, 309
16. Folatelli, G., Contreras, C., Phillips, M. M., Woosley, S. E., Blinnikov, S., Morrell, N., et al. 2006, ApJ, 641, 1039
17. Fruchter, A. S., Levan, A. J., Strolger, L., Vreeswijk, P. M., Thorsett, S. E., Bersier, D., et al. 2006, Nature, 441, 463
18. Galama, T. J., Vreeswijk, P. M., van Paradijs, J., Kouveliotou, C., Augusteijn, T., Böhnhardt, H., et al. 1998, Nature, 395, 670
19. Gal-Yam, A. 2012, Science, 337, 927
20. Gal-Yam, A., Arcavi, I., Ofek, E. O., Ben-Ami, S., Cenko, S. B., Kasliwal, M. M., et al. 2014, Nature, 509, 471
21. Ghisellini, G., Ghirlanda, G., & Tavecchio, F. 2007, MNRAS, 375, L36
22. Gorosabel, J., Larionov, V., & Castro-Tirado, A. J., Guziy, S., Larionova, L., Del Olmo, A., et al. 2006, A&A, 459, L33
23. Greiner, J., Mazzali, P. A., Kann, D. A., Krühler, T., Pian, E., Prentice, S., et al. 2015, Nature, 523, 189
24. Hachinger, S., Mazzali, P. A., Taubenberger, S., Hillebrandt, W., Nomoto, K., & Sauer, D. N. 2012, MNRAS, 422, 70
25. Heger, A., Fryer, C. L., Woosley, S. E., Langer, N., & Hartmann, D. H. 2003, ApJ, 591, 288
26. Hoeflich, P., Langer, N., & Duschinger, M. 1993, A&A, 275, L29
27. Immler, S., Brown, P.J., Milne, P., The, L.-S., Petre, R., Gehrels, N., et al. 2006, ApJ, 648, L119

28. Izzard, R. G., Ramirez-Ruiz, E., & Tout, C. A. 2004, MNRAS, 348, 1215
29. Jeffery, D. J., Kirshner, R. P., Challis, P. M., Pun, C. S. J., Filippenko, A. V., Matheson, T., et al. 1994, ApJ, 421, L27
30. Kasen, D., & Plewa, T. 2007, ApJ, 662, 459
31. Kasen, D., & Bildsten, L. 2010, ApJ, 717, 245
32. Kawabata, K. S., Deng, J., Wang, L., Mazzali, P. A., Nomoto, K., Maeda, K., et al. 2003, ApJ, 593, L19
33. Kelly, P. L., Kirshner, R. P., & Pahre, M. 2008, ApJ, 687, 1201
34. Kelly, P. L., & Kirshner, R. P. 2012, ApJ, 759, 107
35. Kelly, P. L., Filippenko, A. V., Modjaz, M., & Kocevski, D. 2014, ApJ, 789, 23
36. Kouveliotou, C., Meegan, C. A., Fishman, G. J., Bhat, N. P., Briggs, M. S., Koshut, T. M., et al. 1993, ApJ, 413, L101
37. Kulkarni, S. R., Frail, D. A., Wieringa, M. H., Ekers, R. D., Sadler, E. M., Wark, R. M., et al. 1998, Nature, 395, 663
38. Leaman, J., Li, W., Chornock, R., & Filippenko, A. V. 2011, MNRAS, 412, 1419
39. Li, W., Leaman, J., Chornock, R., Filippenko, A. V., Poznanski, D., Ganeshalingam, M., et al. 2011, MNRAS, 412, 1441
40. MacFadyen, A. I., & Woosley, S. E. 1999, ApJ, 524, 262
41. Maeda, K., Nakamura, T., Nomoto, K., Mazzali, P. A., Patat, F., & Hachisu, I. 2002, ApJ, 565, 405
42. Maeda, K., Tanaka, M., Nomoto, K., Tominaga, N., Kawabata, K., Mazzali, P. A., et al. 2007, ApJ, 666, 1069
43. Maeda, K., Kawabata, K., Mazzali, P. A., Tanaka, M., Valenti, S., Nomoto, K., et al. 2008, Science, 319, 1220
44. Matheson, T., Filippenko, A. V., Li, W., Leonard, D. C., & Shields, J. C. 2001, AJ, 121, 1648
45. Maurer, J. I., Mazzali, P. A., Deng, J., Filippenko, A. V., Hamuy, M., Kirshner, R. P., et al. 2010, MNRAS, 402, 161
46. Mazzali, P. A., Nomoto, K., Patat, F., & Maeda, K. 2001, ApJ, 559, 1047
47. Mazzali, P. A., Kawabata, K. S., Maeda, K., Nomoto, K., Filippenko, A. V., Ramirez-Ruiz, E., et al. 2005, Science, 308, 1284
48. Mazzali, P. A., Deng, J., Pian, E., Malesani, D., Tominaga, N., Maeda, K., et al. 2006, ApJ, 645, 1323
49. Mazzali, P. A., Foley, R. J., Deng, J., Patat, F., Pian, E., Baade, D., et al. 2007, ApJ, 661, 892
50. Mazzali, P. A., Valenti, S., Della Valle, M., Chincarini, G., Sauer, D. N., Benetti, S., et al. 2008, Science, 321, 1185
51. Mazzali, P. A., Deng, J., Hamuy, M., & Nomoto, K. 2009, ApJ, 703, 1624
52. Mazzali, P. A., Walker, E. S., Pian, E., Tanaka, M., Corsi, A., Hattori, T., & Gal-Yam, A. 2013, MNRAS, 432, 2463
53. Melandri, A., Pian, E., D'Elia, V., D'Avanzo, P., Della Valle, M., Mazzali, P. A., et al. 2014, A&A, 567, A29
54. Mészáros, P. 2002, ARA&A, 40, 137
55. Metzger, B. D., Margalit, B., Kasen, D., & Quataert, E. 2015, MNRAS, 454, 3311
56. Milisavljevic, D., Fesen, R. A., Chevalier, R. A., Kirshner, R. P., Challis, P., & Turatto, M. 2012, ApJ, 751, 25
57. Modjaz, M., Kewley, L., Bloom, J. S., Filippenko, A. V., Perley, D., & Silverman, J. M. 2011, ApJ, 731, L4
58. Modjaz, M., Blondin, S., Kirshner, R. P., Matheson, T., Berlind, P., Bianco, F. B., et al. 2014, AJ, 147, 99
59. Nakamura, T., Mazzali, P. A., Nomoto, K., & Iwamoto, K. 2001, ApJ, 550, 991
60. Nomoto, K., & Hashimoto, M. 1988, Phys. Rep., 163, 13
61. Owocki, S. P., Romero, G. E., Townsend, R. H. D., & Araudo, A. T. 2009, ApJ, 696, 690
62. Patat, F., Cappellaro, E., Danziger, J., Mazzali, P. A., Sollerman, J., Augusteijn, T., et al. 2001, ApJ, 555, 900
63. Pian, E., Amati, L., Antonelli, L. A., Butler, R. C., Costa, E., Cusumano, G., et al. 2000, ApJ, 536, 778

64. Pian, E., Mazzali, P. A., Masetti, N., Ferrero, P., Klose, S., Palazzi, E., et al. 2006, Nature, 442, 1011
65. Pignata, G., Stritzinger, M., Soderberg, A., Mazzali, P. A., Phillips, M. M., Morrell, N., et al. 2011, ApJ, 728, 14
66. Prentice, S. J,, Mazzali, P. A., Pian, E., Gal-Yam, A., Kulkarni, S. R., Rubin, A., et al. 2016, MNRAS, 458, 2973
67. Pritchard, T. A., Roming, P. W. A., Brown, P. J., Bayless, A. J., & Frey, L. H. 2014, ApJ, 787, 157
68. Sakamoto, T., Hullinger, D., Sato, G., Yamazaki, R., Barbier, L., Barthelmy, S. D., et al. 2008, ApJ, 679, 570
69. Smartt, S. J. 2009, ARA&A, 47, 63
70. Smith, N. J. 2014, ARA&A, 52, 487
71. Soderberg, A. M., Nakar, E., Berger, E., & Kulkarni, S. R. 2006, ApJ, 638, 930
72. Soderberg, A. M., Berger, E., Page, K. L., Schady, P., Parrent, J., Pooley, D., et al. 2008, Nature, 453, 469
73. Starling, R. L. C., Wiersema, K., Levan, A. J., Sakamoto, T., Bersier, D., Goldoni, P., et al. 2011, MNRAS, 411, 2792
74. Tanaka, M., Kawabata, K. S., Maeda, K., Iye, M., Hattori, T., Pian, E., et al. 2009, ApJ, 699, 1119
75. Taubenberger, S., Pastorello, A., Mazzali, P. A., Valenti, S., Pignata, G., Sauer, D. N., et al. 2006, MNRAS, 371, 1459
76. Usov, V. V. 1992, Nature, 357, 472
77. Waxman, E., Mészáros, P., & Campana, S. 2007, ApJ, 667, 351
78. Woosley, S. E., & Bloom, J. S. 2006, ARA&A, 44, 507
79. Woosley, S. E. 2010, ApJ, 719, L204
80. Yaron, O., & Gal-Yam, A. 2012, PASP, 124, 668

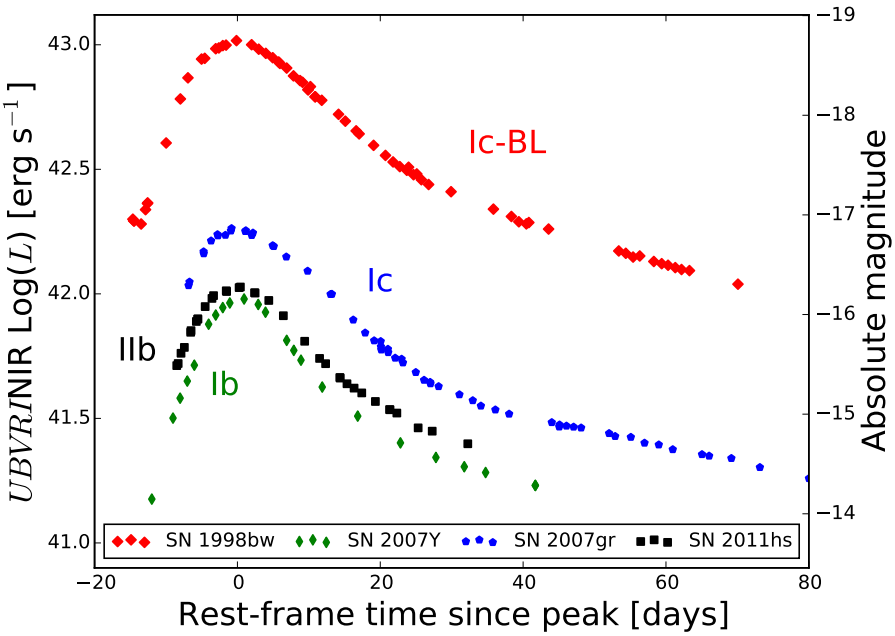

Fig. 1 Pseudo-bolometric light curves of representative stripped-envelope core-collapse SNe of different types based on observations with optical and near-infrared filters.

Acknowledgements We thank Simon Prentice for producing Figures 1 and 2 (left panel), and Avishay Gal-Yam and Iair Arcavi for constructive inputs. The following figures were reprinted with permission: Figure 11 from "The metamorphosis of SN 1998bw", by F. Patat et al., ApJ, vol. 555, year 2001, pages 900-917 (DOI: 10.1086/321526); Figure 3 from "Long gamma-ray bursts and Type Ic core-collapse supernovae have similar locations in hosts", by P. Kelly et al., ApJ, vol. 687, year 2008, pages 1201-1207 (DOI: 10.1086/591925); Figure 4 from "Keck and European Southern Observatory Very Large Telescope view of the symmetry of the ejecta of the XRF/SN 2006aj", by P.A. Mazzali et al., ApJ, vol. 661, year 2007, pages 892-898 (DOI: 10.1086/517912).

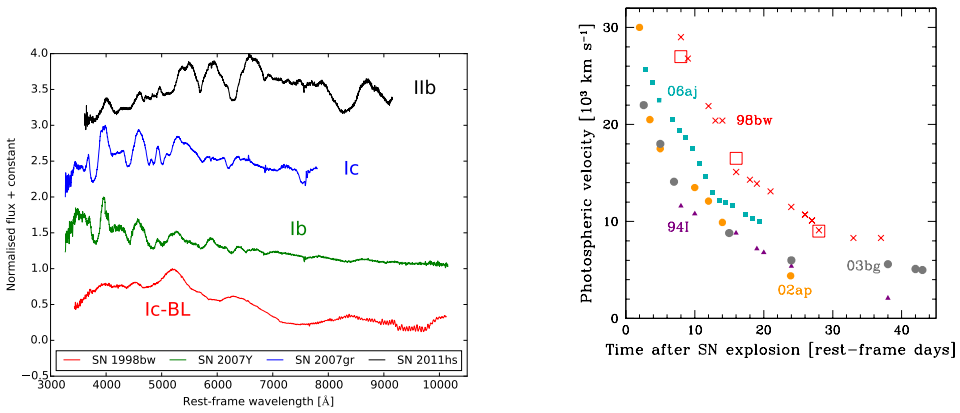

Fig. 2 *Left panel:* Optical spectra of representative stripped-envelope core-collapse SNe of different types. *Right panel:* Temporal evolution of the photosphere expansion velocity of Ic and IIb SNe: normal Ic SN 1994I (purple triangles), broad-lined Ic SN 2002ap (yellow circles) and IIb SN 2003bg (grey circles), GRB SNe 1998w (red crosses and open squares: the former represent measurements made directly on the spectra, the latter are from models) and 2006aj (turquoise squares). See details in Patat et al. (2001), Pian et al. (2006), and Mazzali et al. (2009).

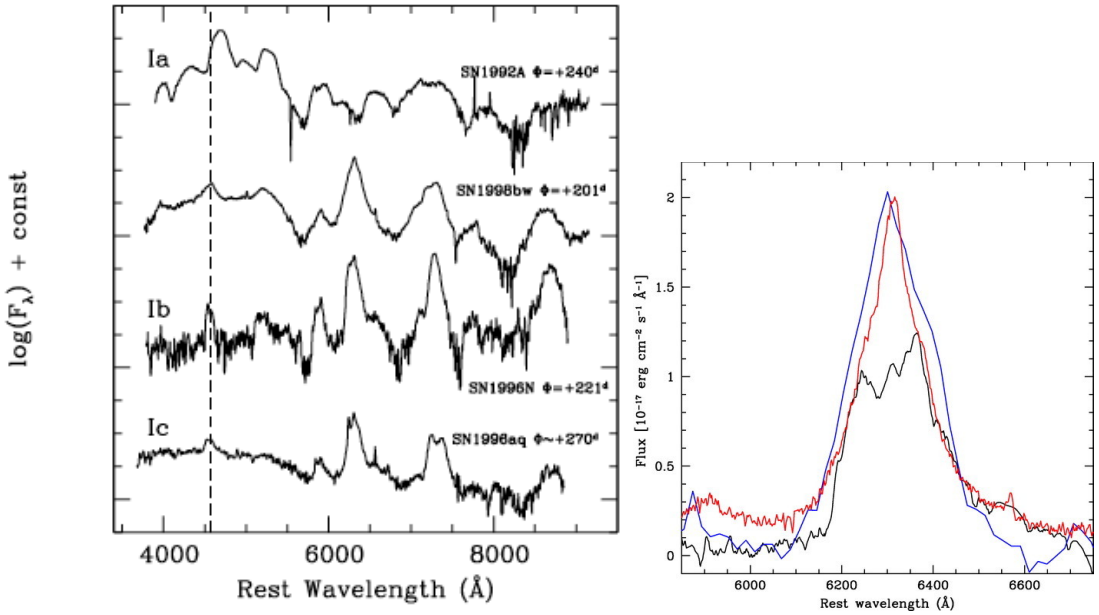

Fig. 3 *Left panel:* Comparison of spectra of SNe 1992A (Ia), 1998bw (broad-lined Ic associated with a GRB), 1996N (Ib), and 1996aq (Ic) at late epochs. The vertical dashed line is placed at the rest-frame wavelength of Mg I] λ4571 (from Patat et al. 2001, ©AAS. Reproduced with permission). Note that the bright [O I] $\lambda\lambda$ 6300, 6363 emission line that is commonly observed in core-collapse SNe in nebular phase is generally absent in Ia SNe. *Right panel:* Comparison of the [O I] $\lambda\lambda$ 6300, 6363 line of SNe 2006aj (blue line), 1998bw (red line; Patat et al. 2001), and 2003jd (black line; Mazzali et al. 2005). The profile of the line in SN 2006aj is less peaked than that of SN 1998bw, although the average expansion velocity of other elements is larger in SN 1998bw than in SN 2006aj, indicating a smaller degree of asphericity in SN 2006aj (from Mazzali et al. 2007, ©AAS. Reproduced with permission).

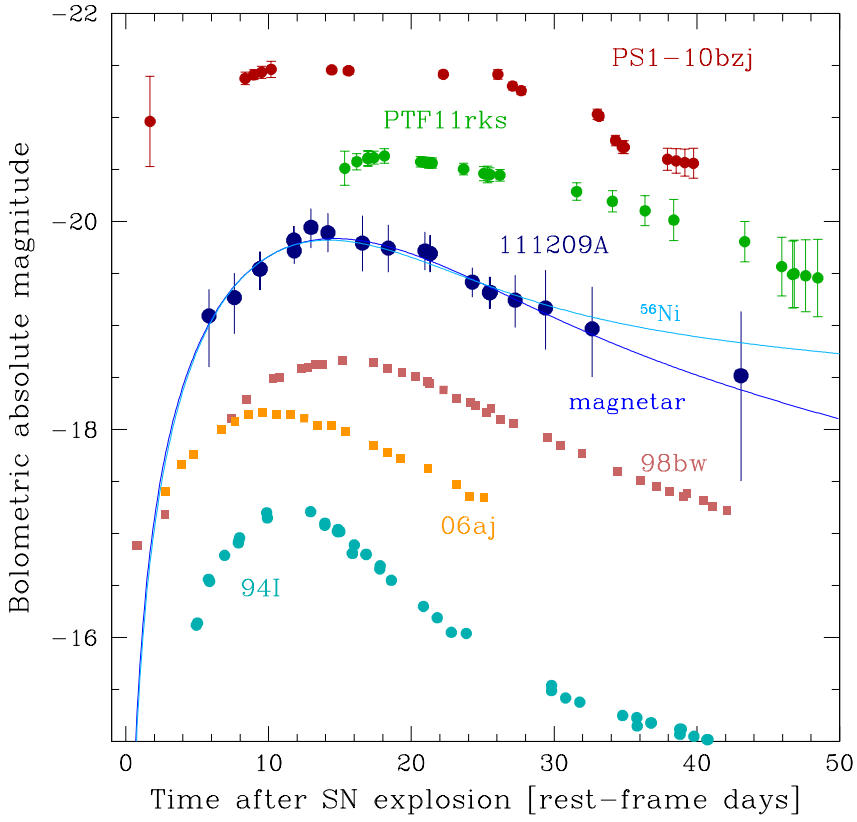

Fig. 4 Bolometric light curves of the "classical" GRB SNe GRB980425/SN 1998bw and X-ray flash 060218/SN 2006aj, the standard type Ic SN 1994I, the hydrogen-poor super-luminous SNe PTF11rks and PS1-10bzj, and the SN 2011kl associated with the ultra-long GRB111209A (observed duration of ∼10000 seconds). SN 2011kl has an intermediate maximum luminosity between the GRB SNe and the super-luminous SNe. Solid lines show the best-fitting synthetic light curves computed with a magnetar injection model (dark blue) and ^{56}Ni powering (light blue). See Greiner et al. (2015) for further details and references.

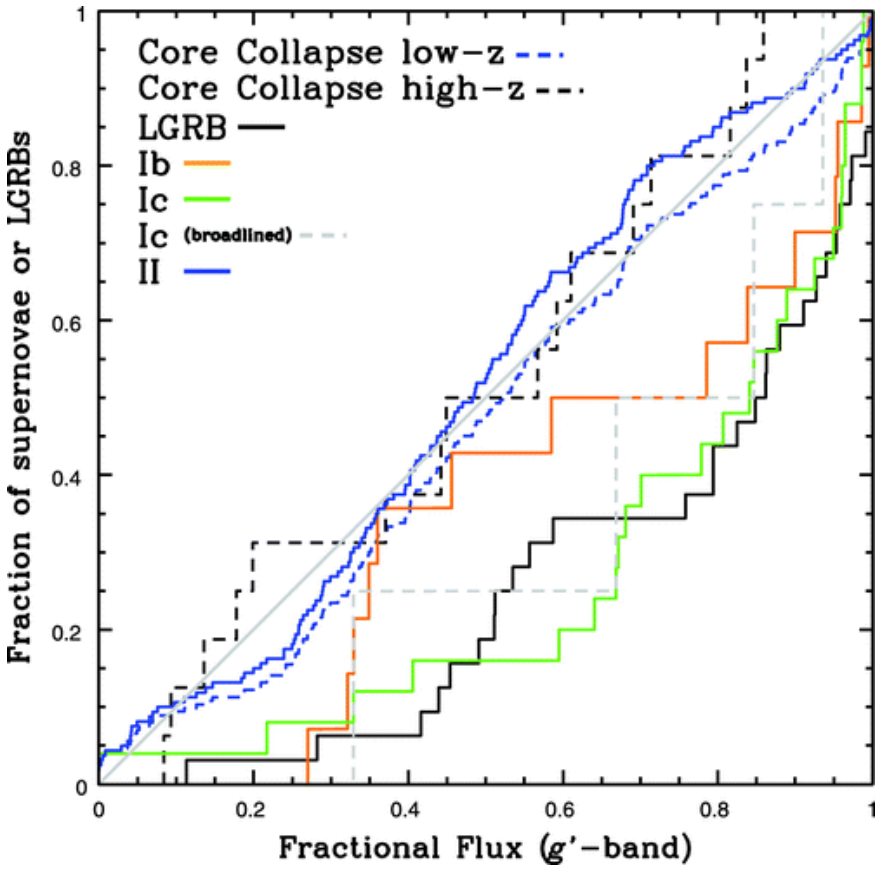

Fig. 5 Bulge-subtracted low-redshift SN g'-band and high-redshift core-collapse SNe and long GRB fractional flux distributions. After removing the bulge light that is present in low-redshift SN hosts but not in the high-redshift and irregular long GRB hosts, there is a high probability ($p = 0.66$) that the SN Ic ($N = 25$, including broad-lined) and the long GRB ($N = 32$) distributions are drawn from the same set. In contrast, it is highly unlikely that SNe II ($N = 160$) and long GRBs are drawn from the same set ($p = 4 \times 10^{-6}$). Bulge subtraction in SN II hosts does not strongly affect the SN II distribution, which remains linear and in good agreement with high-redshift core-collapse SN ($N = 16$; $p = 0.76$). There is a 30% probability that the SN Ib ($N = 14$) distribution is identical to the long GRB distribution, and a 20% probability that it is identical to the Ic distribution (from Kelly et al. 2008, ©AAS. Reproduced with permission).